Magnetic and velocity fluctuation measurements in the REPUTE-1 reversed-field pinch plasma

Akira Ejiri,[a] Satoshi Ohdachi, Toshihiro Oikawa, Shunjiro Shinohara,[b] Kenichi Yamagishi, Hiroshi Toyama, and Kenro Miyamoto[c]
Department of Physics, Faculty of Science, University of Tokyo 7-3-1 Hongo, Bunkyo-ku, Tokyo 113, Japan

(Received 12 July 1993; accepted 20 December 1993)

Magnetic and velocity fluctuations are studied in the REPUTE-1 [Plasma Phys. Controlled Fusion **28**, 805 (1986)] reversed-field pinch (RFP). The first measurement of velocity fluctuation in an RFP plasma has been done using a Doppler shift of the O V(O^{4+}, 278.1 nm) line. The fluctuation level increases as the radius of the viewing chord increases. Magnetic fluctuation measurements by an insertable probe reveal that the radial cross correlation of toroidal field fluctuation changes its sign at the radius slightly inside the reversal surface. The level of magnetohydrodynamic dynamo term is estimated from magnetic fluctuations at the surface correlation changes and oxygen velocity fluctuations measured with the chord distance of 115 mm. The dynamo term and that due to resistivity are the same level. This fact is consistent with Ohm's law on which magnetohydrodynamic dynamo models are based.

I. INTRODUCTION

The equilibrium configuration of the reversed-field pinch (RFP) plasma is basically described by the fully relaxed minimum-energy state developed by Taylor.[1] Since there is no external electric field to sustain the RFP configuration against the resistive diffusion of magnetic fields, there must be some action to sustain the configuration. This action is known as the RFP dynamo. Although this dynamo has been studied for more than a decade, its mechanism and effects remain poorly understood. There are three classes of dynamo models. One is the magnetohydrodynamic (MHD) dynamo model[2–5] and the others are the kinetic dynamo model[6,7] and the tangled discharge model.[8] While the MHD dynamo and the tangled discharge model use the local Ohm's law, the kinetic dynamo model puts emphasis on radial electron diffusion and does not use the local Ohm's law. The MHD dynamo model treats a plasma as an MHD fluid. In this class magnetic and velocity fluctuations play important roles. Many edge magnetic fluctuation measurements have been done and they are qualitatively not inconsistent with the MHD dynamo models, which predict the periodic relaxation of a plasma to the minimum energy state through nonlinear couplings of unstable MHD modes. Recently, the time evolution of perturbation modes has been measured and the nonlinear couplings of these modes were suggested.[9] Periodic relaxations of the q profile have been measured by insertable magnetic probes when the plasma current is low.[10,11] For high plasma current discharges soft-x-ray emissivity becomes large, so that the tomography of soft-x-ray emissivity can be used,[12] and a periodic relaxation is shown. The contours of soft-x-ray emissivity are thought to represent magnetic surfaces. In contrast to the magnetic fluctuation measurements, there is no measurement of the velocity fluctuation before this work.

The MHD dynamo models are based on the local Ohm's law

$$\eta \mathbf{j} = \mathbf{E} + \mathbf{v} \times \mathbf{B}, \tag{1}$$

where η and $\mathbf{j}$ are resistivity and current density, respectively, $\mathbf{E}$ and $\mathbf{B}$ are the vectors of electric and magnetic fields, and $\mathbf{v}$ is the velocity of the plasma. The time averaged poloidal component of this equation is written as

$$\langle \eta j_p \rangle = \langle E_p \rangle + \langle \tilde{\mathbf{v}} \times \tilde{\mathbf{B}} \rangle_p. \tag{2}$$

Since in steady state the time averaged poloidal electric field vanishes, the term $\langle \tilde{\mathbf{v}} \times \tilde{\mathbf{B}} \rangle_p$, which is called as the dynamo term, must be equal to the resistive diffusion term $\langle \eta j_p \rangle$. In order to check the MHD dynamo models, we must measure the velocity fluctuation. The velocity fluctuation may also be responsible for transport and ion heating.

The kinetic dynamo models belong to another class in which the local Ohm's law [Eq. (1)] is not valid. In these models, a low level of magnetic field stochasticity allows the electrons, which are accelerated at the central region of the plasma, to be transported across the mean magnetic field to the edge region.[13] Thus, the electrons sustain the poloidal current at the edge region. The term due to this radial transport (diffusion) of electrons replaces the MHD dynamo term in Eq. (2). Some recent observations of high energy electrons or asymmetric heat flux at the edge of plasma in many RFP's suggest the existence of the radial transport of electrons which is responsible for the kinetic dynamo models.[14–20]

It is important to determine which class of dynamo exists in the RFP plasmas. We report here the results of magnetic and velocity fluctuation measurements in an RFP plasma, and we estimate the level of the dynamo term. It is estimated from the measured magnetic and oxygen velocity

[a]Present address: National Institute for Fusion Science, Nagoya 464-01, Japan.
[b]Present address: Interdisciplinary Graduate School of Engineering Sciences, Kyushu University, Kasuga, Fukuoka 816, Japan.
[c]Present address: Department of Applied Physics, Faculty of Engineering, Seikei University, Musashino-shi, Tokyo 180, Japan.

 1070-664X/94/1(5)/1177/9/$6.00 © 1994 American Institute of Physics

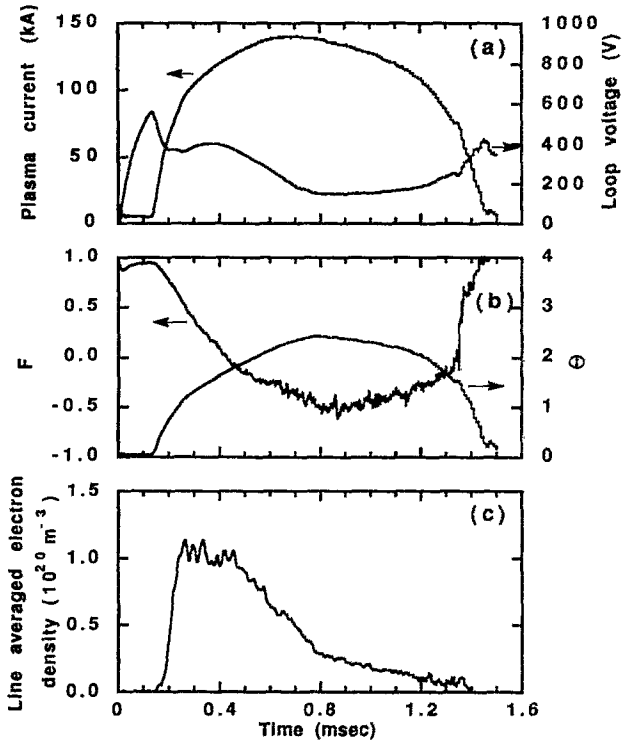

FIG. 1. Time behavior of plasma current, loop voltage (a), F and Θ (b), and line averaged electron density (c).

fluctuations. To measure the magnetic fluctuation level in the plasma and to find how the flux generation occurs an insertable probe is used. The velocity fluctuation is measured from the Doppler shift of O V using a visible spectrometer. To estimate the resistivity electron temperature is measured by a multipoint Thomson scattering system. The level of the dynamo term and the resistive term are estimated and compared.

In Sec. II, the macroscopic behavior of the plasma and the property of magnetic fluctuations are described. In Sec. III, velocity fluctuation measurements are presented. In Sec. IV, Ohm's law is checked using the experimental result. The validity of MHD dynamo models are discussed.

II. TYPICAL DISCHARGE AND MAGNETIC FLUCTUATIONS

The REPUTE-1 RFP device[21] has a toroidal vacuum vessel of major radius 0.82 m and minor radius 0.22 m. The vacuum vessel is surrounded by a stainless steel shell which has a penetration time for the vertical field of 1 ms. The discharges analyzed in this work have a plasma current of 140 kA. The data around $t=0.7$ ms (which is approximately the time when the plasma current reaches the maximum value) are used. Typical time behavior of the plasma parameters are shown in Fig. 1. The reversal parameter F is about -0.5 and the pinch parameter Θ is about 2.3 at $t=0.7$ ms. The line averaged electron density decreases after the setting up phase of an RFP configuration. In order to distinguish the relaxation phenomena from the slow time variation of the equilibrium configuration, we

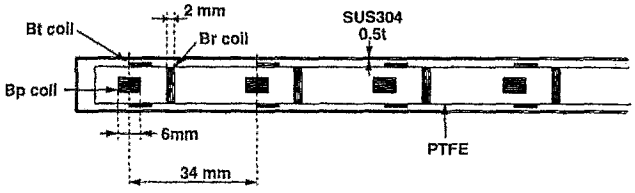

FIG. 2. Schematic view of the magnetic probe. It measures B_t, B_p, and B_r at four radial positions. The coils are covered with SUS protective jacket.

use a numerical frequency filter ($\geqslant$5 kHz). When we calculate a level (RMS) of fluctuation, the trend and average are subtracted.

The insertable magnetic probe consists of 12 pickup coils which can measure toroidal, poloidal, and radial magnetic fields at four radial positions simultaneously (Fig. 2). These coils are covered with a stainless steal protective jacket, and their frequency response is about 40 kHz (-3 dB). In contrast to other RFP devices, the heat load to inserted probes or to targets is relatively small.[17] The probe can be inserted almost into the center of the plasma without affecting macroscopic plasma parameters. The probe is scanned radially and rotated by a movable probe system.

Power spectra of magnetic fluctuations measured by the insertable magnetic probe and that measured by pickup coils just inside the vacuum vessel show peaks at 10–20 kHz. These dominant magnetic fluctuations are recognized as periodic relaxations of a plasma to the near-minimum-energy state.[10,11]

Absolute fluctuation levels increases as the radius decreases. We define the relative level of fluctuation as the ratio of RMS of fluctuation to the time averaged (0.6–0.8 ms) magnetic field strength at the same position. Figure 3 shows the relative levels of the magnetic fluctuation as a function of radius. The relative level of toroidal field fluctuation decreases as the radius decreases. The relative level of poloidal field fluctuation slightly increases as the radius decreases. The relative level of radial field fluctuation has a peak around $r=100$–150 mm.

Since the dynamo generates the toroidal flux, the toroidal field fluctuation is a good indicator of it. As shown in Fig. 4, the toroidal field fluctuations at the inner region of the plasma are in antiphase with that at the outer region. These toroidal fluctuations are accompanied by periodic relaxations which show the oscillation of the safety factor on axis.[10] The radial and poloidal fluctuations at different radii show almost no phase difference.

The surface where the radial correlation of toroidal field fluctuation changes its sign is, subsequently, called the correlation-reversal surface. The average radius of the surface is calculated from cross-correlation coefficients. The cross-correlation coefficient between two time series $x(t)$, $y(t)$ with the time delay of τ is defined as $R_{xy}(\tau) = C_{xy}(\tau)/\sqrt{C_x(0)C_y(0)}$, where $C_x(0)$ and $C_y(0)$ are autocorrelation functions with zero-time delay, and $C_{xy}(\tau)$ is a cross-correlation function.

The cross-correlation coefficient has a maximum or a

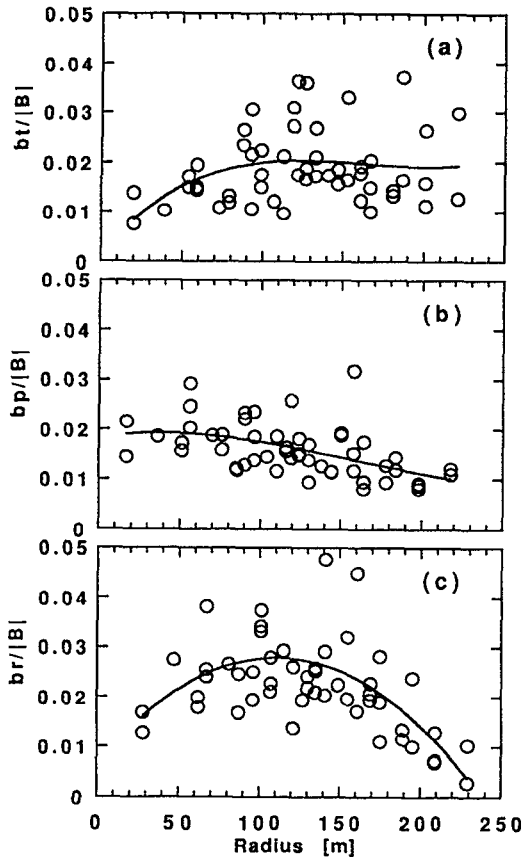

FIG. 3. Radial profiles of the relative level of magnetic fluctuations. Toroidal (a), poloidal (b), and radial (c) field fluctuations are shown.

minimum at zero-time delay. Hence, we use the coefficients with zero-time delay. In order to determine the average correlation-reversal surface, we plot in Fig. 5 the cross-correlation coefficient with zero-time delay as a function of radial position and of radial separation. The coefficients are averaged over about 40 discharges. The cross-correlation

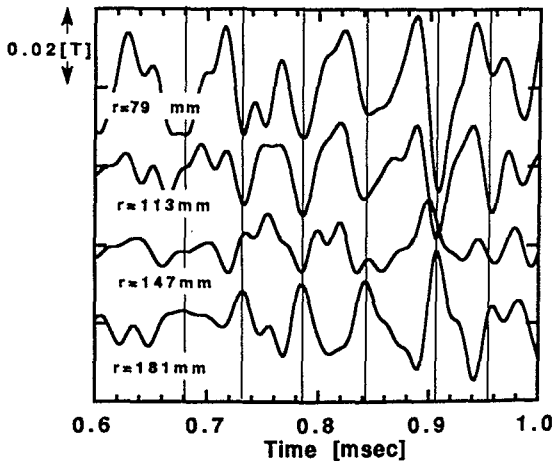

FIG. 4. Toroidal field fluctuations (5–50 kHz) at four radial positions (r=79 mm, r=113 mm, r=147 mm, r=181 mm). Straight lines are guides to see the relation between fluctuations.

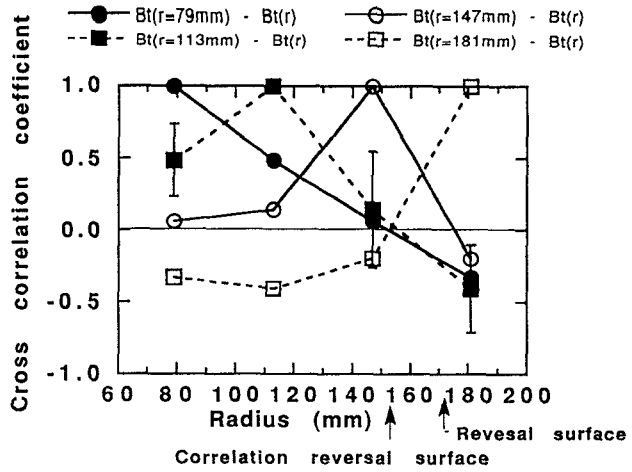

FIG. 5. Cross-correlation coefficient of toroidal field fluctuation as a function of radial separation and of radial position. The closed circle denotes cross-correlation function for $bt(r=79$ mm) and $bt(r)$, closed square for $bt(r=113$ mm) and $bt(r)$, open circle for $bt(r=147$ mm) and $bt(r)$, open square for $bt(r=181$ mm) and $bt(r)$.

coefficients of toroidal field fluctuation show that the average correlation-reversal surface exists at $r\approx 150$ mm, which is slightly inside the reversal surface at $r\approx 170$ mm.

We can also calculate the radial correlation lengths of magnetic fluctuations from cross-correlation coefficients. The correlation length $\lambda_x(r)$ of a fluctuation $x(t,r_i)$ is defined as

$$\lambda_x\left(\frac{r_i+r_{i+1}}{2}\right)=\frac{\Delta r}{R_{x(r_i)x(r_{i+1})}(0)}, \tag{3}$$

where $x(r_i)$, $x(r_{i+1})$ are the signals of two neighboring coils. This correlation length corresponds to the e-folding length of the cross-correlation coefficient. Figure 6 shows the profiles $\lambda_x(r)$ of toroidal, poloidal, and radial field fluctuations. The error bars represent the shot by shot deviations. The large shot by shot deviations are due to the short duration of averaging, which is 0.2 ms. The correlation length of toroidal field fluctuation decreases towards the correlation-reversal surface as the radius increases, and the correlation length of poloidal field fluctuation slightly increases and that of radial field fluctuation seems to be flat. The average correlation length is about 40 mm. These results are consistent with those in ETA-BETA II.[22,23]

The radial mode pattern of magnetic fluctuations are measured in the Ohmically Heated Toroidal Experiment (OHTE),[24,25] High Beta Toroidal Experiment 1A (HBTX1A),[26,27] and in STE-2.[28,29] In these devices the toroidal field fluctuation of the mode changes its sign slightly inside the reversal surface, and the poloidal one also changes its sign at the more inner radius. Similarity between the observed patterns and the calculated $m=1$ resistive internal kink (tearing) modes was shown. In contrast to their results, in REPUTE-1 and ETA-BETA II,[23] the radial phase relation of the poloidal field does not show the change of its sign. In REPUTE-1, the high frequency (>40 kHz) component of poloidal field fluctuation, of which power is small, seems to change the sign. The exist-

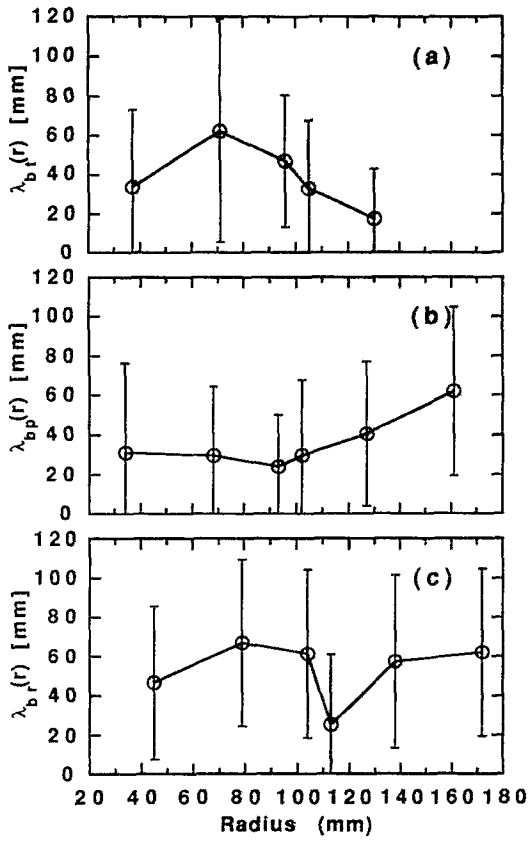

FIG. 6. Correlation length of toroidal (a), poloidal (b), and radial (c) field as a function of radius. The error bars denote the shot by shot deviation.

ence of several modes during a relaxation period makes it difficult to compare the experiments with theories directly.

III. MEASUREMENTS WITH VISIBLE SPECTROMETER

A. Visible spectrometer

The visible spectrometer system has been installed at a horizontal port and it views a chord in a poloidal cross section. The distance of the viewing chord from the plasma center is scanned by a mirror from -115 to $+115$ mm (Fig. 7). The width of the viewing sight is about 20 mm at the plasma center. Scanning the mirror shot by shot, the

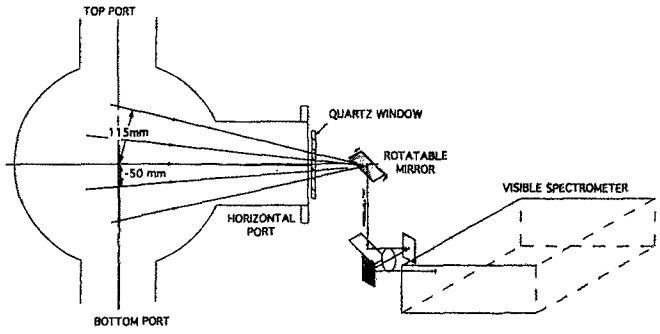

FIG. 7. Viewing sight of the visible spectrometer system.

profile of temperature, velocity, intensity, and fluctuations of these quantities are measured. The frequency response of the system is up to $2\pi/RC \approx 17$ kHz (-3 dB), where R, C are resistance and capacitance of the preamplifier of a photomultiplier tube (PMT), respectively. The spectrometer has eight PMT's.

Measured Doppler broadening of a line is fitted to a Maxwellian distribution, by a nonlinear least-square method. The fitting function Y_j for jth channel is written as

$$Y_j=\frac{I_i I_j}{\sqrt{\pi}}\left(\frac{2T_i\lambda_0^2}{m_i c^2}+\frac{\Delta\lambda_{1/2j}^2}{4\log(2)}\right)^{-1/2} \times\exp\left[-\left(\lambda_j-\lambda_0-\frac{v_i}{c}\lambda_0\right)^2\left(\frac{2T_i\lambda_0^2}{m_i c^2}+\frac{\Delta\lambda_{1/2j}^2}{4\log(2)}\right)^{-1}\right], \tag{4}$$

where I_j, λ_j, and $\Delta\lambda_{1/2j}$ are the relative sensitivity, central wavelength, and full width at half-maximum (FWHM) of the jth channel. Free parameters of this function is temperature T_i, velocity v_i, and total intensity I_i. The parameters are determined to minimize $S=\Sigma_{j=1}^{8}(y_j-Y_j)^2/\sigma_j^2$, where σ_j is the error the of jth channel signal. The error of the signal consists of quantum noise, errors in relative sensitivity, electromagnetic noise, and bit noise in analog-to-digital (A/D) conversion. Among these errors, the quantum noise is dominant. The error of fitting parameters is calculated from the error of the signal of each channel, using the propagation law of errors. For example, the error of temperature is calculated as $\Delta T_i=[\Sigma_{j=1}^{8}(\partial T_i/\partial\sigma_j)^2\sigma_j^2]^{1/2}$. Thus, the errors of the fitting parameter are coupled through these kinds of equations. The correlations between errors of parameter such as $|\Delta T_i\Delta v_i|/\sqrt{\Delta T_i}\sqrt{\Delta v_i}$ are about 0.1. Since each parameter represents a different feature of the Maxwellian distribution, correlations between errors are small when the data fits well to a Maxwellian distribution function.

Random errors of the measured velocity create spurious velocity fluctuations and affect the velocity fluctuation levels. It is important to estimate the error accurately to subtract the effect of random errors from the observed velocity fluctuations. When we measure velocity fluctuation levels, we neglect the errors in the relative sensitivity, because the error is not random and does not fluctuate during a discharge, and its effect on the velocity fluctuation levels is very small.

Here, we will describe the process to determine the quantum noise. Since the quantum noise obeys the Poisson process, we need to know the number of photons detected by a detector to determine the quantum noise. At first, the statistical property of the signals of a detector when a single photon is detected is investigated. Second, using this statistical property, the quantum noise is calculated as a function of the time integral of a signal. The calculated relative noise is $1/\sqrt{N}$, where N is the number of detected photon in an integration time. This $1/\sqrt{N}$ dependence is a characteristic of the Poisson process. Finally, the light of a mercury lamp is used as a source of light and the deviation

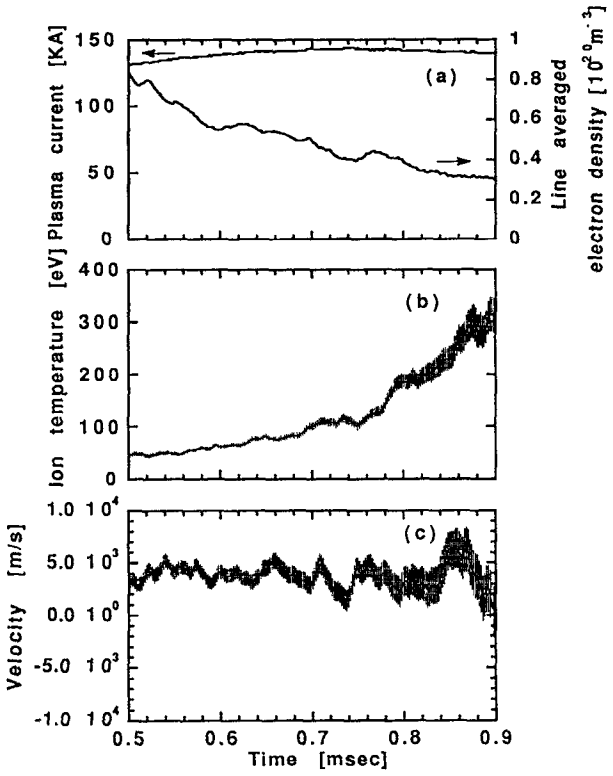

FIG. 8. Time evolution of plasma current and line averaged electron density (a), temperature (b), and velocity (c) of O V (278.1 nm). The chord distance is 0 mm. The absolute velocity cannot be measured accurately.

of a signal from its average is measured as a function of the time integral of the signal. It coincides well with the calculated quantum noise. The last method has been used to calibrate Thomson scattering systems.[30,31] As a result we can calculate the quantum noise for a given signal.

Among observed lines of impurities, O V(O^{4+}, 278.1 nm) is used for the measurements of temperature and velocity. The intensity of O V is strong in the discharges with the plasma current lower than about 200 kA.

The time evolution of the temperature and velocity of O V are shown in Fig. 8. In most discharges, the temperature increases toward the end of a discharge, while the line averaged electron density decreases or is constant. The measured spectrum fits well to a single Maxwellian distribution except at the terminating phase of a discharge. The normalized $\chi^2[=S/(8-3)]$ is about 1 before the terminating phase. At the terminating phase, the spectrum fits better to a bi-Maxwellian distribution, which has six fitting parameters. The bi-Maxwellian distribution has a high temperature component and a low temperature component. The low temperature probably represents the edge low temperature due to the influx of impurities from the wall.

The measured value contains the information along the viewing chord. Figure 9 shows the time averaged intensity of the O V (278.1 nm) line as a function of the chord distance. The error bar represents the shot by shot deviation of about 50 shots. The distance is defined to be negative when the spectrometer views the lower side of the torus and defined to be positive when it views the upper side. Since the intensity profile is broad, the poloidal structure with high poloidal mode numbers would be averaged and would not contribute to the measured values. The temperature profile is flat within the range of measurements (-115–$+115$ mm). The possible effect of the edge low temperature is strongest around the peak in a spectrum. In order to see the effect of the edge low temperature, which cannot be measured directly, we did the fitting without two central channels. The measured temperature is slightly larger for this (six-channel) fitting compared with the eight-channel fitting. As described later, the oxygen velocity fluctuation levels are obtained by subtracting the effect of random errors from the observed velocity fluctuation. The six-channel fitting shows larger velocity fluctuations and larger random errors, and the resultant oxygen velocity fluctuation levels are approximately the same as those for the eight-channel fitting. These facts show that the viewing sight averaged measurements represent the global values rather than the local values, but does not represent edge values.

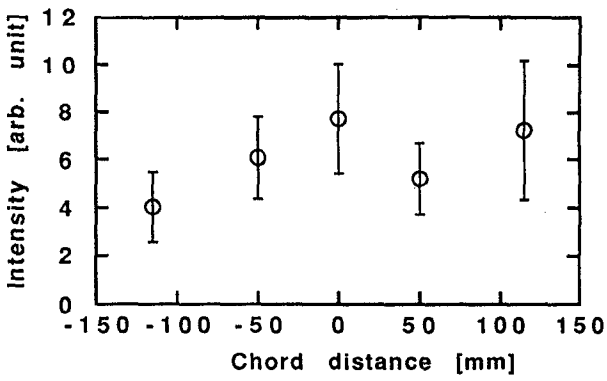

FIG. 9. Intensity of O V (278.1 nm) as a function of the chord distance.

B. Velocity fluctuation measurements

When the spectrometer views the lower or upper side of the torus, a large velocity fluctuation with the frequency of 10–20 kHz is observed. Figure 10 shows an example of the Doppler broadening of O V (278.1 nm) with the chord distance of 115 mm. The solid curves represent fitted curves to single Maxwellian distributions. Figure 11 shows the time evolution of the velocity fluctuation. The observed velocity fluctuation is much larger than the error bars.

The fluctuation contains not only the oxygen velocity fluctuation but also the fluctuation due to random errors of the observed velocity. The observed velocity $v_{\rm raw}$ is

$$v_{\rm raw}=v_{O^{4+}}+\Delta v, \tag{5}$$

where $v_{O^{4+}}$ and Δv are the oxygen velocity and its error, respectively. The error of the velocity is calculated from the error of the signal using the propagation law of error. The error of the signal mainly comes from the quantum noise of the PMT. The quantum noise depends on the time

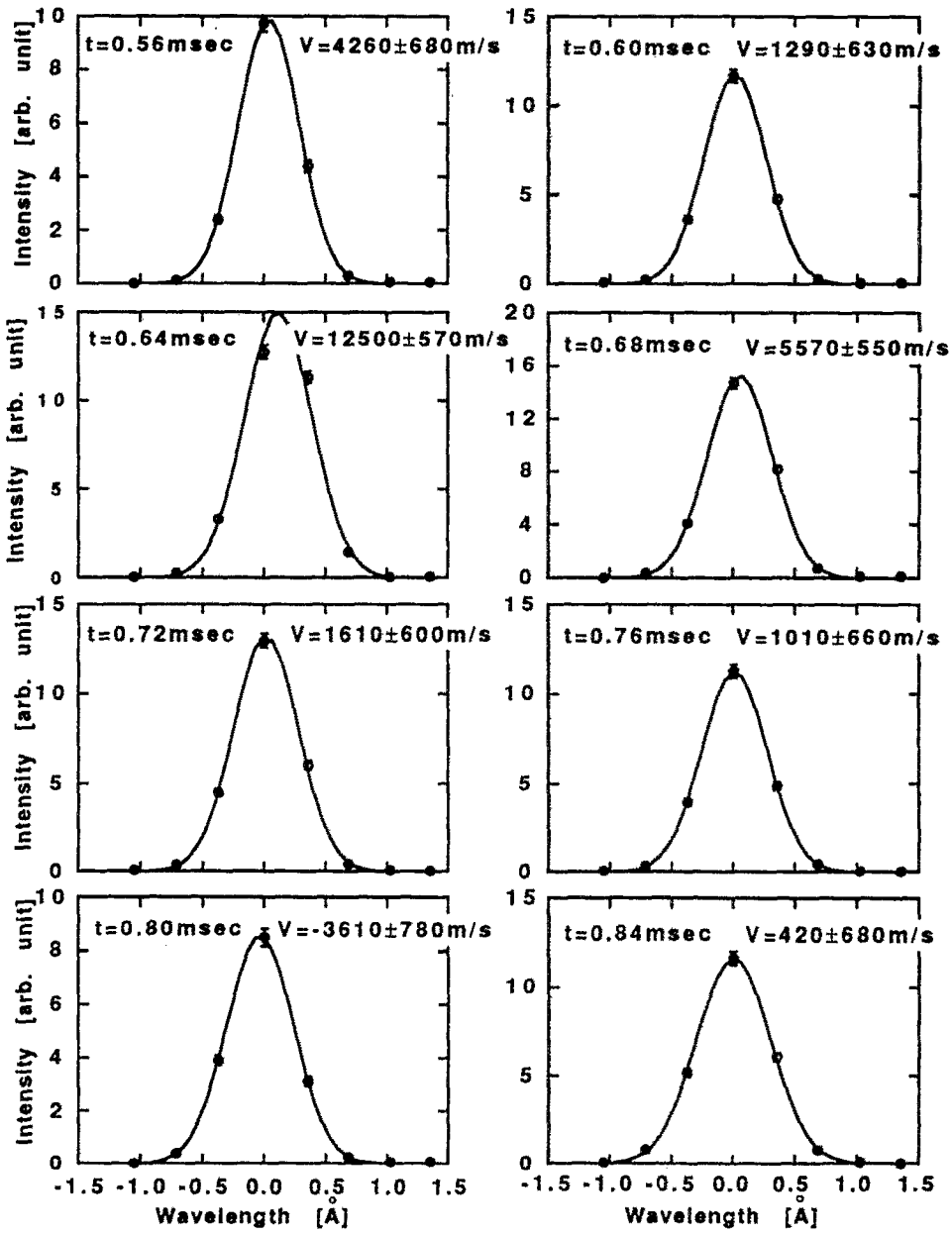

FIG. 10. Doppler broadening of O v (278.1 nm) for various times. Solid curve represents a single Maxwellian distribution. The chord distance is 115 mm.

of numerical smoothing. A typical smoothing time is 6 μs, which is comparable to the decay time of 10 μs for a single photon signal.

The time averaged velocity is written as

$$\langle v_{\rm raw}\rangle = \langle v_{O^{4+}}\rangle + \langle \Delta v\rangle \approx \langle v_{O^{4+}}\rangle, \tag{6}$$

where $\langle\ \rangle$ represents the time averaging. $\langle \Delta v\rangle$ can be neglected because the averaging time period (0.3 ms) is long enough to reduce the quantum noise. The observed velocity fluctuation $\widetilde{v_{\rm raw}}$ is

$$\widetilde{v_{\rm raw}} = v_{\rm raw} - \langle v_{\rm raw}\rangle \approx v_{O^{4+}} + \Delta v - \langle v_{O^{4+}}\rangle \approx \widetilde{v_{O^{4+}}} + \Delta v, \tag{7}$$

where $\widetilde{v_{O^{4+}}} \equiv v_{O^{4+}} - \langle v_{O^{4+}}\rangle$ is the oxygen velocity fluctuation. Observed fluctuation level is written as

$$\langle \widetilde{v_{\rm raw}}^2\rangle \approx \langle \widetilde{v_{O^{4+}}}^2\rangle + 2\langle \widetilde{v_{O^{4+}}}\rangle\langle \Delta v\rangle + \langle \Delta v^2\rangle \approx \langle \widetilde{v_{O^{4+}}}^2\rangle + \langle \Delta v^2\rangle. \tag{8}$$

Since the probability of the error of velocity obeys a Gaussian distribution (except in the case where the number of detected photon is too small), the ensemble average of the square of the error $[\Delta v^2]$ corresponds to half of the square of 1σ of the Gaussian distribution $1/2\Delta v_G^2$. We assume that shot averaging and the time averaging have the role of ensemble averaging. The duration of the time averaging is 0.3 ms. The ensemble averaged oxygen fluctuation level $[\widetilde{v_{O^{4+}}}^2]$ can be written as

$$[\widetilde{v_{O^{4+}}}^2] = [\widetilde{v_{\rm raw}}^2] - [\Delta v^2] = [\widetilde{v_{\rm raw}}^2] - [\tfrac{1}{2}\Delta v_G^2]. \tag{9}$$

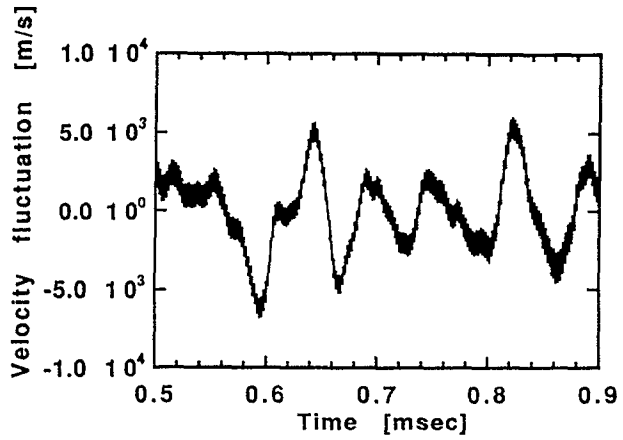

FIG. 11. Time evolution of velocity fluctuation calculated from the Doppler shift of O V (278.1 nm). The chord distance is 115 mm.

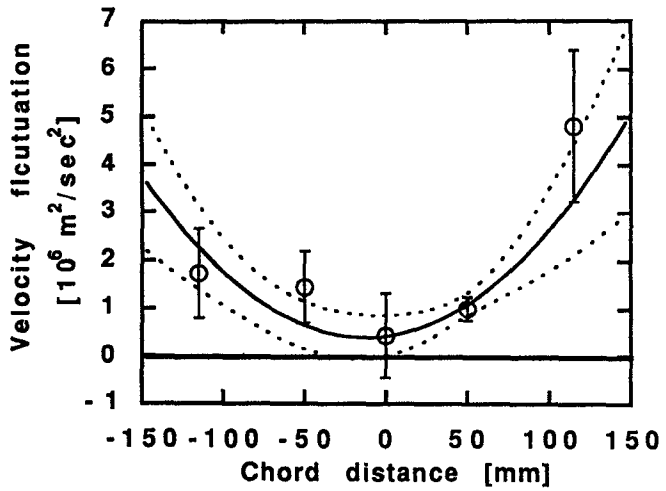

FIG. 12. Oxygen velocity fluctuation measured by the Doppler shift of O V (278.1 nm) as a function of chord distance. The error bars represent shot by shot deviation. The solid curve represents the fitting to the second-order polynomial.

Figure 12 shows the fluctuation level of the oxygen velocity calculated from Eq. (9) as a function of the chord distance. The fluctuation level seems to have a minimum around the center and it increases as (the absolute value of) the chord distance increases. If the plasma rotates without shear, the velocity and its fluctuation are linear functions of the radius. In this case, the square of them are proportional to the square of the radius. The velocity fluctuation level fits well to the second-order polynomial (solid curve) within the range of the error bars.

The dotted curves in Fig. 12 represent the region of $\pm 1\sigma$ error. We can conclude that the velocity fluctuation has a minimum around the center and it increases as the chord distance increases, but we cannot determine whether the minimum velocity fluctuation level is finite or not because of the large shot by shot deviation. The velocity fluctuation level with the chord distance of ± 115 mm is about 3×10^6 m^2/s^2. Since the profile of the intensity is broad (Fig. 9) the measured fluctuation represents the global motion of the impurity.

It is not obvious that impurities and bulk ions have the same velocity. If the momentum coupling between impurities and bulk ions is strong, they would have the same velocity. The equation of motion of component i is written as

$$\frac{d\mathbf{V}_i}{dt}=-\frac{1}{n_i m_i}\nabla p_i+\frac{eZ}{m_i}(\mathbf{E}+\mathbf{V}_i\times\mathbf{B})-\frac{\mathbf{R}_i}{n_i m_i}, \qquad (10)$$

where $\mathbf{R}_i$ is the drag by other species. Since we are going to discuss the phenomena related to the relaxation processes, which has a frequency of 10–20 kHz, DC components can be rejected in the following discussions. DC components contribute to the DC velocity or the continuously increasing or decreasing velocity, which appears as a trend in velocity. The trend is excluded when we calculate fluctuation levels. The contribution of each term can be represented by the time scale, and the term with the smallest time scale controls the impurity motion. The time scale of the drag is the slowing-down time, which is written as $\tau_S=-V/(\mathbf{R}_i/n_i m_i)$, where τ_S is the slowing-down time. Suppose that the velocity difference between bulk ions and impurities is the same order as the oxygen velocity fluctuation levels. Since the velocity fluctuation levels are smaller than the oxygen thermal velocity and much smaller than the hydrogen (bulk ion) thermal velocity, the slowing-down time is a function of the bulk ion temperature and density. It is about 20 μs for the bulk ion with the temperature of 100 eV and the density of 0.5×10^{20} cm^{-3}.

The second term in Eq. (10) is $eZ/m_i(\mathbf{E}+\mathbf{V}_i\times\mathbf{B})$ which is roughly about a factor 4 ($=m_i/Z$) smaller than $e/m_{\text{bulk}}(\mathbf{E}+\mathbf{V}_{\text{bulk}}\times\mathbf{B})$. The latter term is related to current driven instabilities, which is thought to be dominant in RFP plasmas. Since the time scale of the fluctuations in our plasmas is about 50–100 μs, the time scale due to the second term is probably much larger than the slowing-down time.

The first term in Eq. (10) is the force due to the pressure gradient. Suppose we have a case with 100 eV temperature difference along the poloidal direction with a frequency of 10–20 kHz. Then the time scale could be 1 μs. However this case might be too extreme, and the real time scale might be much longer. Thus, we conclude that the oxygen velocity fluctuations probably represents that of bulk ions.

IV. DISCUSSION AND CONCLUSION

Using the oxygen velocity fluctuation levels and some assumptions here, we will check the local Ohm's law. We consider the Ohm's law at the correlation-reversal surface, where the flux generation seems to occur. Because of the broad intensity profile of O V and the relatively long radial correlation length of the magnetic fluctuations, the observed velocity fluctuation with the chord distance of 115 mm is approximately the same level as that at of the correlation-reversal surface. The phase relation between $\tilde{v}$ and $\tilde{B}$ at the same point is not measured. Thus, we can only estimate the absolute level of the dynamo term.

The poloidal component of the dynamo term is $\tilde{v}_r\tilde{B}_t-\tilde{v}_t\tilde{B}_r$. We assume that we can neglect the first term at the correlation-reversal surface. The ratio of poloidal velocity to the toroidal one depends on the poloidal and toroidal mode numbers of the fluctuation of the plasma motion. The soft-x-ray tomography results with a plasma current of 200 kA show $m=1$ deformation in a poloidal cross section and suggest $m=1$ poloidal motion.[21] The soft-x-ray tomography at two poloidal cross sections shows that fluctuations are almost resonant to the local field.[32] Therefore, the plasma motion is roughly perpendicular to the local fields. This geometrical configuration can be caused by the helical reconnection lines suggested in simulations with single helicity.[5,33] In these simulations the plasma flows towards a helical line and causes a magnetic reconnection at this line, and the radial fields and the velocity flow perpendicular to the helical reconnection line which contribute to the flux generation. The velocity flow with $m=1$ is also shown in another simulation.[34]

If the mode of the plasma motion is resonant to the field on axis, this ratio is $R/r_sq_0\approx 0.6$–0.8, where R and q_0 are the major radius and safety factor on axis, respectively, and r_s is the radius of the correlation-reversal surface. Thus, we assume the toroidal velocity fluctuation and the measured fluctuation level are the same level. Then the dynamo term is written as

$$|\tilde{v}_t||\tilde{B}_r| \sim |\widetilde{v_{O^{4+}}}||\tilde{B}_r| \sim \sqrt{3\times 10^6}[\mathrm{m/s}]\times 0.0075[\mathrm{T}]\approx 13[\mathrm{V/m}]. \quad (11)$$

Here, $|\widetilde{v_{O^{4+}}}|$ is the measured value with the chord distance of 115 mm, and $|\tilde{B}_r|$ is the amplitude of radial fluctuation measured by the insertable magnetic probe. This magnetic fluctuation amplitude is about 5% of the mean magnetic field.

Resistivity η is estimated from the electron temperature by the use of Spitzer resistivity

$$5.2\times 10^{-5}Z_{\mathrm{eff}}\log\Lambda T_e^{-3/2}[\Omega\mathrm{m}], \quad (12)$$

where T_e is the electron temperature in electron-volts, Z_{eff} is a mean ion charge, and $\log\Lambda\approx 15$ is the Coulomb logarithm. The electron temperature profile (Fig. 13) has been measured by a multipoint Thomson scattering system. The shot averaged electron temperature profile is approximated by the following function:

$$T_e(r)\approx 46[1-(r/a)^2] \quad [\mathrm{eV}], \quad (13)$$

where a is the minor radius. In ZT-40M, when T_e is low (≈ 100 eV), Z_{eff} is lower than about 2.[35] In ETA-BETA II, it is about 1, except at the edge plasma.[36] Although Z_{eff} is not measured in REPUTE-1, it is assumed to be 2. Then the resistive diffusion term is written as

$$\langle\eta j\rangle_p\approx 12[\mathrm{V/m}]. \quad (14)$$

Here, the current density j is calculated using the modified Bessel function model.[37]

The level of the resistive diffusion term can be estimated from another method. If dynamo bursts occur as observed in the Madison Symmetric Torus (MST) device,[38] the toroidal flux decays continuously and the flux generation occurs as bursts. The decay rate of continuous decay phase represents the poloidal voltage due to the resistive diffusion. We can measure the fluctuation of the poloidal voltage at the edge. In REPUTE-1, the measured poloidal voltage at the edge shows fluctuation, of which the amplitude is about 3 V and the frequency is 10–20 kHz. The poloidal voltage due to the previously estimated resistive diffusion term is $2\pi r_s\langle\eta j\rangle_{\mathrm{res}}\approx 12$ V. $r_s\approx 150$ mm is the radius where the flux generation and the diffusion are assumed to balance. This is three times larger than the measured poloidal voltage at the edge. One of the reasons that explains this difference is that the fluctuation of the toroidal flux at the edge may be affected by the existence of the vacuum vessel and resistive shell. The other reason is that the flux generation in REPUTE-1 does not show bursts. Therefore, the simultaneous diffusion and flux generation reduce the fluctuation of the toroidal flux. Also the transport of the generated or consumed flux at the edge region of the plasma will obscure the fluctuation measured at the plasma boundary. We can conclude that the estimated resistive diffusion term at $r_s\approx 150$ mm is not inconsistent with the toroidal flux fluctuation measured at the edge.

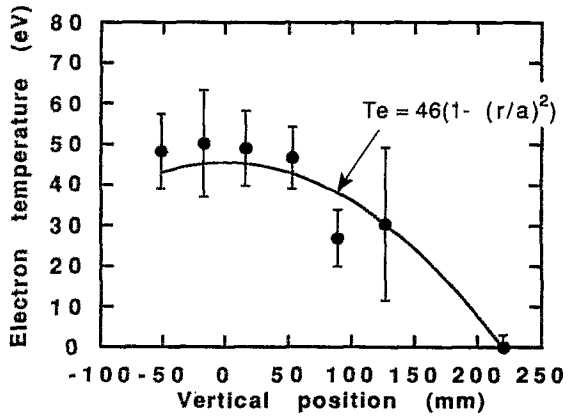

FIG. 13. Electron temperature profile measured by Thomson scattering system. The error bars denote the average error of the measured temperature. An artificial point (at 220 mm) is added to calculate the temperature profile (solid line) by the least-square method.

Comparing Eq. (11) and Eq. (14) shows that both terms are the same level. Although there are many assumptions, the oxygen velocity fluctuation level suggests the existence of an appropriate dynamo term, which is required for the MHD dynamo in the REPUTE-1 RFP plasma.

The MHD dynamo term can be estimated by electrostatic and magnetic probes. The estimated MHD dynamo term at the edge region of the REPUTE-1 RFP plasma is small and suggests the kinetic dynamo term.[20] But the MHD dynamo term around $r\sim 150$ mm can be sufficient for the required dynamo term in the estimation (Fig. 4 in Ref. 20). It is possible that the MHD dynamo sustains the RFP configuration at the inner region and the kinetic dynamo sustains it at the edge region.

In the kinetic dynamo model, the stochastic diffusion term is assumed to be much larger than the collision term for the fast electrons.[39] When the electron–ion collision

term is dominant, we can use the local Ohm's law. The stochastic diffusion term for the fast electrons with parallel velocity v_F is written as

$$\left.\frac{\partial f}{\partial t}\right|_{st} = \frac{|v_F|}{r}\frac{\partial}{\partial r}\left(rD_M\frac{\partial f}{\partial r}\right), \tag{15}$$

where D_M is the magnetic diffusivity. It is written as $D_M = L_r(b_r/B_0)^2$, where L_r is the parallel correlation length of radial field fluctuations. At the plasma edge L_r is about 0.35 m,[20] but it is difficult to measure L_r in the plasma. We assume that the correlation length of the soft-x-ray emissivity is the same as L_r. The correlation between soft-x-ray fluctuations at two poloidal cross sections has been measured.[32] It is about 0.15 at the radius of $r=0.12$ m and with the poloidal angle difference corresponding to the $m=1$, $n=8$ mode. The e-folding correlation length is about 0.46 m. This gives $D_M/a \sim 1.9\times10^{-3}$ m. From Eq. (15), the time scale for the stochastic diffusion is $ra/(v_F D_M)$. This scale is about 15 μs for the electron with the velocity of $\sqrt{100\ \text{eV}/m_e}$. The time scale of electron–ion collision is $\lesssim 1$ μm in the plasma with the density of $0.5\times10^{20}\ \text{m}^{-3}$. Thus, for electrons with energy comparable to the central temperature (~ 50 eV) we can use the local Ohm's law. Thus, the approach of the kinetic dynamo model is not good around a radius of $r=0.12$ m. Further discussions including the estimation of the energy and amount of fast electrons is beyond the scope of the present article.

In conclusion, we have found that the average correlation-reversal surface of toroidal field fluctuation exists slightly inside the reversal surface. If we assume resistive diffusion of the toroidal flux and flux generation due to the MHD dynamo term balance at this surface, the measured velocity fluctuation level of O^{4+} (O V) is enough to account for the flux generation. This fact supports the MHD dynamo models.

ACKNOWLEDGMENTS

The authors wish to thank N. Asakura for his help in the calibration system of the visible spectrometer. They would also like to thank Y. Nagayama for help in the Thomson scattering measurements. One of the authors (AE) wishes to acknowledge useful discussions with A. Fujisawa and Y. Shimazu.

[1] J. B. Taylor, Phys. Rev. Lett. **33**, 139 (1974).
[2] A. Y. Aydemir and D. C. Barnes, Phys. Rev. Lett. **52**, 930 (1984).
[3] D. D. Schnack, E. J. Caramana, and R. A. Nebel, Phys. Fluids **28**, 321 (1985).
[4] E. J. Caramana and D. D. Schnack, Phys. Fluids **29**, 3023 (1986).
[5] K. Kusano and T. Sato, Nucl. Fusion **27**, 821 (1987).
[6] A. R. Jacobson and R. W. Moses, Phys. Rev. A **29**, 3335 (1984).
[7] R. W. Moses, K. F. Schoenberg, and D. A. Baker, Phys. Fluids **31**, 3152 (1988).
[8] M. G. Rusbridge, Plasma Phys. **19**, 499 (1977).
[9] K. Hattori, Y. Hirano, T. Shimada, Y. Yagi, I. Hirota, and K. Ogawa, Phys. Fluids B **3**, 3111 (1991).
[10] Y. Ueda, N. Asakura, S. Matsuzuka, K. Yamagishi, S. Shinohara, Y. Nagayama, H. Toyama, K. Miyamoto, and N. Inoue, Nucl. Fusion **27**, 1453 (1987).
[11] V. Antoni, P. Martin, and S. Ortolani, Nucl. Fusion **29**, 1759 (1989).
[12] N. Asakura, Y. Nagayama, S. Shinohara, H. Toyama, and K. Miyamoto, Nucl. Fusion **29**, 893 (1989).
[13] A. B. Rechester and M. N. Rosenbluth, Phys. Rev. Lett. **40**, 38 (1978).
[14] J. C. Ingraham, R. F. Ellis, J. N. Downing, C. P. Munson, P. G. Weber, and G. A. Wurden, Phys. Fluids B **2**, 143 (1990).
[15] Y. Yagi, T. Shimada, I. Hirota, Y. Maejima, Y. Hirano, K. Ogawa, K. Namiki, and K. Ioki, J. Nucl. Mater. **162–164**, 702 (1989).
[16] Y. Yagi, T. Shimada Y. Hirano, K. Hattori, Y. Maejima, I. Hirota, K. Saito, and S. Shiina, in *Proceedings of the 17th European Conference on Controlled Fusion and Plasma Heating*, Amsterdam, 1990 (European Physical Society, London, 1990), Vol. 2, p. 545.
[17] A. Ejiri (private communication, 1990).
[18] V. Antoni, M. Bagatin, D. Desideri, E. Martines, and Y. Yagi, in *Proceedings of the 18th European Conference on Controlled Fusion and Plasma Physics*, Berlin, 1991 (European Physical Society, London, 1991), Vol 3, p. 69.
[19] Y. Yagi, Y. Hirano, T. Shimada, K. Hattori, Y. Maejima, I. Hirota, and A. A. Newton, Plasma Phys. Controlled Fusion **33**, 1391 (1991).
[20] H. Ji, H. Toyama, A. Fujisawa, S. Shinohara, and K. Miyamoto, Phys. Rev. Lett. **69**, 616 (1992).
[21] N. Asakura, T. Fujita, K. Hattori, N. Inoue, S. Ishida, K. Kamada, S. Mattsuzuka, K. Miyamoto, J. Morikawa, Y. Nagayama, H. Nihei, S. Shinohara, H. Toyama, Y. Ueda, K. Yamagishi, and Z. Yoshida, Plasma Phys. Controlled Fusion **28**, 805 (1986).
[22] V. Antoni, M. Bassan, A. Buffa, S. Costa, L. Giudicotti, W. Grossmann, S. Martini, S. Ortolani, R. Paccagnella, M. E. Puiatti, S. Scarin, M. Valisa, and E. Zilli, in *Plasma Physics Cotrolled Nuclear Fusion Research 1984* (International Atomic Energy Agency, Vienna, 1985), Vol. 2, p. 487.
[23] V. Antoni and S. Ortolani, Plasma Phys. **25**, 799 (1983).
[24] R. R. Goforth T. N. Carlstrom, C. Chu, B. Curwen, D. Graumann, P. S. C. Lee, E. J. Nilles, T. Ohkawa, M. J. Schaffer, T. Tamano, P. L. Taylor, T. S. Taylor, and D. F. Register, Nucl. Fusion **26**, 515 (1986).
[25] R. J. La Haye, T. N. Carlstron, R. R. Goforth, G. L. Jackson, M. J. Schaffer, T. Tamano, and P. L. Taylor, Phys. Fluids **27**, 2576 (1984).
[26] H. A. B. Bodin, C. A. Bunting, P. G. Carolan, L. Giudicotti, C. W. Gowers, Y. Hirano, I. H. Hutchinson, P. A. Jones, C. Lamb, M. Malacarne, A. A. Newton, V. A. Piotrowicz, T. Shimada, and M. R. C. Watts, in *Plasma Physics Controlled Nuclear Fusion Research 1982* (International Atomic Energy Agency, Vienna, 1983), Vol. 1, p. 641.
[27] P. G. Caloran, B. Alper, M. K. Bevir, H. A. B. Bodin, D. R. Brotherton-Ratcliffe, H. Ahmed, D. E. Evans, D. Evans, A. R. Field, L. Firth, M. J. Forrest, C. G. Gimblett, N. C. Hawkes, I. H. Hutchinson, M. Malacarne, A. Manley, A. A. Newton, P. G. Noonan, A. Patel, N. J. Peacock, D. P. Storey, H. Tsui, and P. D. Wilcock, in *Plasma Physics Controlled Nuclear Fusion Research 1984* (International Atomic Energy Agency, Vienna, 1985), Vol. 2, p. 449.
[28] S. Koh and H. Oshiyama, J. Phys. Soc. Jpn. **55**, 2901 (1986).
[29] S. Masamune, K. Kawasaki, A. Murata, D. Ishijima, M. Iida, and H. Oshiyama, Plasma Phys. Controlled Fusion **35**, 209 (1993).
[30] T. Yamauchi and JFT-2M Experimental Group, Jpn. J. Appl. Phys. **28**, L707 (1989).
[31] S. Ohdachi, Master thesis, University of Tokyo, 1991 (in Japanese).
[32] Y. Shimazu, Ph.D. thesis, University of Tokyo, 1992.
[33] R. Horiuchi and T. Sato, Phys. Fluids **31**, 1142 (1988).
[34] E. J. Caramana, R. A. Nebel, and D. D. Schnack, Phys. Fluids **26**, 1305 (1983).
[35] P. G. Weber, Phys. Fluids **28**, 3136 (1985).
[36] L. Gabellieri, M. Giubbilei, S. Martin, S. Ortolani, M. E. Puiatti, and P. Scarin, Nucl. Fusion **27**, 863 (1987).
[37] K. F. Schoenberg, R. F. Gribble, and J. A. Phillips, Nucl. Fusion **22**, 1433 (1982).
[38] S. Hokin, A. Almagri, S. Assadi, J. Beckstead, G. Chartas, N. Crocker, M. Cudzinovic, D. Den Hartog, R. Dexter, D. Holly, S. Prager, T. Rempel, J. Sarff, E. Scime, W. Shen, C. Spragins, C. Sprott, G. Starr, M. Stoneking, and C. Watts, Phys. Fluids B **3**, 2241 (1991).
[39] K. F. Schoenberg and R. W. Moses, Jr., Phys. Fluids B **3**, 1467 (1991).